Subtractive Patterning via Chemical Lift-Off Lithography

Wei-Ssu Liao *et al.*

Science **337**, 1517 (2012);
DOI: 10.1126/science.1221774

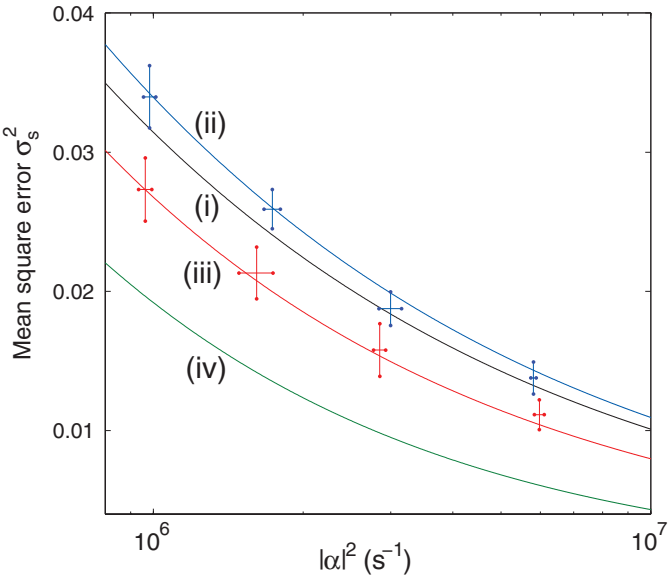

Fig. 4. Dependence of the smoothed MSE σ_s^2 on the amplitude squared $|\alpha|^2$. Blue and red crosses are experimental data for coherent and squeezed beams, respectively. Trace (i) is the coherent-state limit. Trace (ii) is the theoretical curve for coherent beams with the experimental setup (i.e., including inefficiency). Trace (iii) is the theoretical curve for squeezed beams, including inefficiency. Trace (iv) is the theoretical curve for pure squeezed beams and 100% efficiency, with the squeezing level optimized for each $|\alpha|^2$.

Experimentally, we varied the amplitude $|\alpha|$ while fixing the pump beam power to 80 mW, giving squeezing and antisqueezing levels of -3.2 ± 0.2 dB and 4.9 ± 0.3 dB, respectively. Theoretically, the optimal squeezing level increases with $|\alpha|$, and so too does the squeezing enhancement, without limit. However, for our experimental conditions ($10^6\ s^{-1} \leq |\alpha|^2 < 10^7\ s^{-1}$) the effect of keeping the squeezing fixed is minor (less than 3% difference to σ_s^2). Figure 4 shows the dependence of the MSE σ_s^2 on $|\alpha|$. The theoretical curves show good agreement with experiments. Over the whole amplitude range, the estimates with the squeezed beams surpass what is possible with coherent states, with σ_s^2, averaged over the four different amplitudes, being $15 \pm 4\%$ below the CSL. The conclusion is essentially unaltered if one calculates the CSL not in terms of $|\alpha|^2$ but in terms of the effective photon flux $\mathcal{N}_{\text{eff}}$, which equals $|\alpha|^2$ plus the extra photons resulting from the squeezed vacuum fluctuations in the relevant spectral range (*26*).

We have tracked the phase of a squeezed optical field that varies stochastically in time over a substantial angular range. Our use of Kalman filtering in real-time adaptive measurements of nonclassical systems could be applied also in solid-state and nanomechanical devices. Optimizing both the degree of squeezing and its bandwidth according to the experimental conditions would allow a completely rigorous treatment of photon flux. Lower losses and more squeezing would then enable a dramatic improvement to a precision that scales differently with photon flux, with $\sigma^2 \propto \mathcal{N}^{-5/8}$ (*20*) as opposed to the $\sigma^2 \propto \mathcal{N}^{-1/2}$ in the current setup.

References and Notes

1. R. Slavík *et al.*, *Nat. Photonics* **4**, 690 (2010).
2. J. Chen, J. L. Habif, Z. Dutton, R. Lazarus, S. Guha, *Nat. Photonics* **6**, 374 (2012).
3. V. Giovannetti, S. Lloyd, L. Maccone, *Nat. Photonics* **5**, 222 (2011).
4. C. W. Helstrom, *Quantum Detection and Estimation Theory* (Academic Press, New York, 1976).
5. V. Giovannetti, S. Lloyd, L. Maccone, *Science* **306**, 1330 (2004).
6. H. M. Wiseman, G. J. Milburn, *Quantum Measurement and Control* (Cambridge University Press, Cambridge, 2010).
7. C. M. Caves, *Phys. Rev. D Part. Fields* **23**, 1693 (1981).
8. K. Goda *et al.*, *Nat. Phys.* **4**, 472 (2008).
9. J. Abadie *et al.*, *Nat. Phys.* **7**, 962 (2011).
10. K. Inoue, E. Waks, Y. Yamamoto, *Phys. Rev. Lett.* **89**, 037902 (2002).
11. G. Y. Xiang, B. L. Higgins, D. W. Berry, H. M. Wiseman, G. J. Pryde, *Nat. Photonics* **5**, 43 (2011).
12. T. Nagata, R. Okamoto, J. L. O'Brien, K. Sasaki, S. Takeuchi, *Science* **316**, 726 (2007).
13. H. M. Wiseman, *Phys. Rev. Lett.* **75**, 4587 (1995).
14. H. M. Wiseman, R. B. Killip, *Phys. Rev. A* **57**, 2169 (1998).
15. D. W. Berry, H. M. Wiseman, *Phys. Rev. Lett.* **85**, 5098 (2000).
16. M. A. Armen, J. K. Au, J. K. Stockton, A. C. Doherty, H. Mabuchi, *Phys. Rev. Lett.* **89**, 133602 (2002).
17. B. L. Higgins, D. W. Berry, S. D. Bartlett, H. M. Wiseman, G. J. Pryde, *Nature* **450**, 393 (2007).
18. A. Hentschel, B. C. Sanders, *Phys. Rev. Lett.* **104**, 063603 (2010).
19. D. W. Berry, H. M. Wiseman, *Phys. Rev. A* **65**, 043803 (2002).
20. D. W. Berry, H. M. Wiseman, *Phys. Rev. A* **73**, 063824 (2006).
21. T. A. Wheatley *et al.*, *Phys. Rev. Lett.* **104**, 093601 (2010).
22. M. Tsang, J. H. Shapiro, S. Lloyd, *Phys. Rev. A* **79**, 053843 (2009).
23. M. Tsang, H. M. Wiseman, C. M. Caves, *Phys. Rev. Lett.* **106**, 090401 (2011).
24. M. Tsang, *Phys. Rev. Lett.* **102**, 250403 (2009).
25. C. W. Gardiner, *Handbook of Stochastic Methods* (Springer, Berlin, 1985).
26. See supplementary materials on *Science* Online.

Acknowledgments: This work was partly supported by Project for Developing Innovation Systems, Grants-in-Aid for Scientific Research, Global Center of Excellence, Advanced Photon Science Alliance, Funding Program for World-Leading Innovative R&D on Science and Technology commissioned by the Ministry of Education, Culture, Sports, Science and Technology (MEXT) of Japan, Strategic Information and Communications R and D Promotion program of the Ministry of Internal Affairs and Communications of Japan, and the Australian Research Council projects CE110001029, DP1094650, and FT100100761.

Supplementary Materials

www.sciencemag.org/cgi/content/full/337/6101/1514/DC1
Materials and Methods
Supplementary Text
Figs. S1 to S8
References (*27–30*)

28 May 2012; accepted 13 August 2012
10.1126/science.1225258

Subtractive Patterning via Chemical Lift-Off Lithography

Wei-Ssu Liao,[1,2] Sarawut Cheunkar,[1,3] Huan H. Cao,[1,2] Heidi R. Bednar,[1,2] Paul S. Weiss,[1,2,3,4,5]* Anne M. Andrews[1,2,6,7]*

Conventional soft-lithography methods involving the transfer of molecular "inks" from polymeric stamps to substrates often encounter micrometer-scale resolution limits due to diffusion of the transferred molecules during printing. We report a "subtractive" stamping process in which silicone rubber stamps, activated by oxygen plasma, selectively remove hydroxyl-terminated alkanethiols from self-assembled monolayers (SAMs) on gold surfaces with high pattern fidelity. The covalent interactions formed at the stamp-substrate interface are sufficiently strong to remove not only alkanethiol molecules but also gold atoms from the substrate. A variety of high-resolution patterned features were fabricated, and stamps were cleaned and reused many times without feature deterioration. The remaining SAM acted as a resist for etching exposed gold features. Monolayer backfilling into the lift-off areas enabled patterned protein capture, and 40-nanometer chemical patterns were achieved.

High-throughput molecular printing strategies with high feature resolution are central goals for lithography. However, progress has been impeded by the conflicting aims of large-area fabrication versus precision, and of convenience versus cost (*1–4*). For instance, although photolithography enables patterning over large areas (centimeters), the prototyping process is time-consuming and resolution is restricted by light diffraction (*1–3*). Patterning by electron beam lithography (EBL) or scanning probe lithography (SPL) techniques, such as dip-pen nanolithography,

nanoshaving, and nanografting (*5*–*7*), produces high-resolution features (<10 nm and <100 nm for EBL and SPL, respectively) (*1*–*3*), but throughput is limited by serial processing speeds.

Soft-lithography strategies produce patterns over large areas at the micro- and nanoscales (*1*, *3*, *4*, *8*–*10*). Commercial polymers (such as polydimethylsiloxane, PDMS) are used as molds for pattern transfer via contact printing. The bas-relief pattern on a master mold is fabricated by photolithography for large-area patterning or EBL for high-resolution patterning (*1*, *3*). Once the master is generated, patterned features are negatively transferred to PDMS stamps, which are then "inked" with organic molecules, proteins, nanoparticles, or DNA (*1*, *10*–*16*).

Among the materials transferred, organic molecules such as alkanethiols and other related molecules, which form self-assembled monolayers (SAMs) on Au substrates, can be readily subjected to chemical modification at the exposed terminal groups for capturing biomolecules (*1*, *16*–*18*). Moreover, SAMs serve as "molecular resists" against different wet etchants, enabling patterns to be transferred reproducibly to underlying substrates (*19*). However, the success of contact printing and related soft-lithography techniques is also limited by the chemistries and compatibility of the inks, stamps, and substrates (*1*, *3*, *4*). For example, lateral diffusion and gas-phase deposition of ink molecules tend to reduce pattern fidelity (*20*, *21*), creating a resolution limit of ~100 nm for alkanethiols on Au.

To overcome the limitations of stamp feature replication in soft lithography, the general principles of contact printing must be modified to achieve sharp, stable, and reproducible chemical features on substrates (*7*, *19*, *22*, *23*). We transformed the conventional contact printing process such that the polymer stamp is activated and then used to lift off a preformed SAM resist. A strong contact-induced interaction at the stamp-SAM interface enables the transfer of sharp stamp features by mechanical desorption of resist only in the areas of stamp-substrate contact. The subtractive nature of this process precisely replicates features from the master mold (*9*, *24*). This approach, chemical lift-off lithography (CLL), facilitates the addition of different molecules into the lift-off areas to produce multicomponent patterned SAMs. It also enables the intact areas to act as an etch resist for the transfer of features to the underlying substrate. Moreover, stamps used for CLL can be cleaned and reused many times without deterioration.

Alkanethiols with different terminal groups (Table 1) were used to form SAMs on Au-coated Si substrates. Soft-lithography stamps were created from PDMS to transfer features of different geometries from master molds (fabricated by standard photolithography and EBL techniques) to the molecular-resist layers (*1*, *8*, *10*). The CLL process is outlined schematically in Fig. 1. A PDMS stamp was first activated by exposure to oxygen plasma, yielding a fully hydrophilic and reactive surface (*17*, *25*–*27*). The stamp and SAM-modified substrate were then brought into conformal contact. The stamp was peeled away from the substrate, which removed resist molecules selectively in the areas contacted by the stamp, transferring stamp features with high resolution to the substrate.

On the basis of earlier work, we hypothesized that the Au-Au bonds in the substrate metal lattice, rather than the Au-S bonds between the substrate and alkanethiol, are preferentially broken during lift-off. The breaking of Au-Au bonds during SAM desorption has been a particular subject of controversy (*6*, *28*–*32*). The mobility of Au thiolates within SAMs (*29*, *33*, *34*) indicates that weak Au-Au bonds are present at the substrate surface. Furthermore, recent studies show the presence of Au adatoms beneath SAMs, which leads to facile Au-Au bond breakage because of reduced coordination of the adatoms (*35*–*38*). We made a featureless, oxygen plasma–treated PDMS stamp and brought it into contact with a hydroxyl-terminated SAM-coated Au surface. After lift-off, a peak indicating the presence of Au was observed on the PDMS stamp surface by x-ray photoelectron spectroscopy (XPS; see spectra in fig. S1). This finding is consistent with Au being removed from the underlying substrate (*39*).

The presence of Au on oxygen plasma–treated PDMS surfaces after chemical lift-off led us to propose that a contact-induced chemical reaction between the hydrophilic stamp surface and the molecular-resist layer results in Au-Au bond rupture during stamp removal. Studies have shown that oxygen plasma treatment yields siloxyl

Table 1. Alkanethiol molecules and terminal groups used in chemical lift-off lithography.

Alkanethiol	Chemical formula
Hydroxyl-terminated tri(ethylene glycol)undecanethiol (TEG)	$HS\text{-}(CH_2)_{11}\text{-}(C_2H_4O)_3\text{-}OH$
Biotin-terminated hexa(ethylene glycol)undecanethiol	$HS\text{-}(CH_2)_{11}\text{-}(C_2H_4O)_6\text{-}NH\text{-}C_{10}H_{15}O_2N_2S$
Hydroxyl-terminated undecanethiol	$HS\text{-}(CH_2)_{11}\text{-}OH$
Methyl-terminated undecanethiol	$HS\text{-}(CH_2)_{11}\text{-}CH_3$
Methoxy-terminated tri(ethylene glycol)undecanethiol	$HS\text{-}(CH_2)_{11}\text{-}(C_2H_4O)_3\text{-}O\text{-}CH_3$

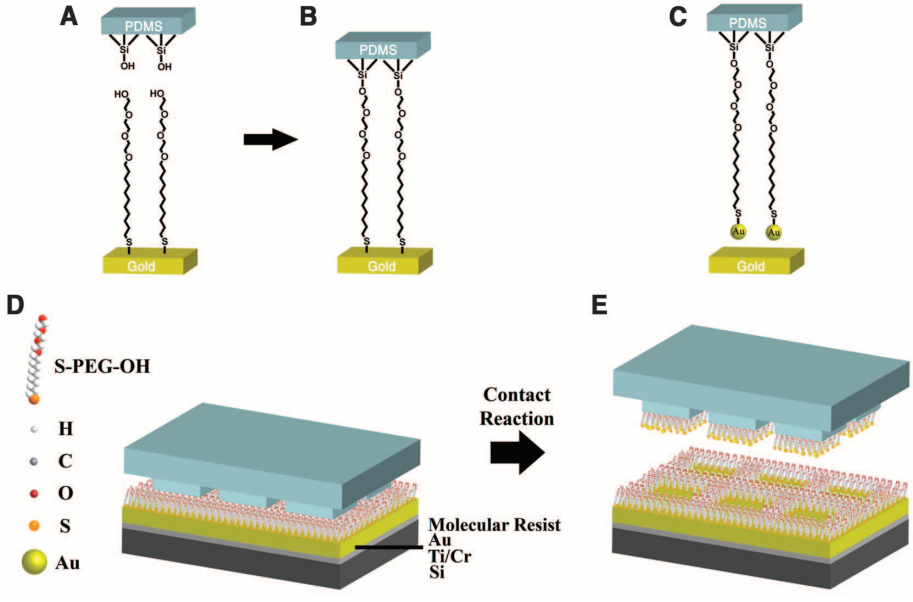

Fig. 1. Schematic illustration of the molecular-resist lift-off process. (**A**) A polydimethylsiloxane (PDMS) stamp is activated by oxygen plasma treatment, producing hydrophilic siloxyl groups. (**B**) A surface-induced contact reaction is implemented via close contact between the stamp and hydroxyl-terminated molecules self-assembled on an Au substrate. (**C**) Stamp removal lifts off resist molecules and underlying Au. (**D**) In chemical lift-off lithography (CLL), a patterned PDMS stamp is brought into conformal contact with a self-assembled molecular resist. (**E**) Lift-off is limited to the stamp-contact regions.

[1]California NanoSystems Institute, University of California, Los Angeles, CA 90095, USA. [2]Department of Chemistry and Biochemistry, University of California, Los Angeles, CA 90095, USA. [3]Department of Chemistry, Pennsylvania State University, University Park, PA 16802, USA. [4]Department of Materials Science and Engineering, University of California, Los Angeles, CA 90095, USA. [5]Department of Physics, Pennsylvania State University, University Park, PA 16802, USA. [6]Department of Psychiatry and Biobehavioral Health, University of California, Los Angeles, CA 90095, USA. [7]Semel Institute for Neuroscience and Human Behavior, University of California, Los Angeles, CA 90095, USA.

*To whom correspondence should be addressed. E-mail: aandrews@mednet.ucla.edu (A.M.A.); psw@cnsi.ucla.edu (P.S.W.)

groups on PDMS stamp surfaces, which facilitate condensation reactions between Si-OH and hydroxyl groups on different oxides, such as Au, Ti, and Si to form Si-O-Au, Si-O-Ti, and Si-O-Si linkages, respectively (*9*, *24*, *40*–*42*). We anticipated that the same type of linkage (Si-O-SAM) would be established between Si-OH groups on oxygen plasma–treated PDMS stamp surfaces and hydroxyl-terminated groups on SAMs.

To investigate the roles of the molecular resist tail groups in the CLL process, we assembled two different hydroxyl-terminated alkanethiol molecules, with and without oligo(ethylene glycol), as molecular resist monolayers (Table 1). Both provided good transfer of stamp features to SAM-coated Au substrates (Fig. 2 and fig. S5A). In contrast, when methoxy- or methyl-terminated alkanethiol molecules (Table 1) were tested under the same assembly and lift-off conditions, no detectable transfer of stamp features was found on SAM-coated Au surfaces (figs. S5B and S5C, respectively). Stamp features were not transferred when a hydrophilic PDMS stamp was used directly with a bare Au substrate (fig. S5D). Thus, tail group reactivity dictates whether lift-off occurs via hydrophilic PDMS stamps.

Fourier-transform infrared reflection absorption spectroscopy (FT-IRRAS) was used to investigate the extent of lift-off occurring in a prototypical SAM. Spectral analysis indicated that 75 to 80% of hydroxyl-terminated undecanethiol molecules are removed after the lift-off process (fig. S6). Previous reactive patterning of hydrogen-bonding SAMs showed that this level of damage makes the SAM labile to complete displacement, and the hydrogen bonding in the intact areas prevents diffusion and thus pattern dissolution (*43*). The terminal functionality of the initial SAM influences lift-off via the extent of the contact-induced reaction at the SAM-stamp interface. Lift-off from SAMs of hydroxyl-terminated tri(ethylene glycol)alkanethiol (TEG) was sufficient to enable patterning of underlying substrates by wet etching and to produce patterned multicomponent SAMs capable of biorecognition (see below).

Chemical patterns of TEG were characterized by atomic force microscopy (AFM) and bright-field optical microscopy, as shown in Figs. 2 and 3. Stamps with depressed well-like motifs or protruding posts were used to create different surface relief patterns. The stamp negative was produced in the resist, as molecules were removed (instead of added) by patterning. For example, islands of SAM resist remained when a stamp with a depressed relief was used; the areas surrounding the relief on the stamp contacted the SAM surface, and the molecular resist was removed in these areas during the lift-off step. The AFM topographic image in Fig. 2A illustrates the protruding SAM islands after patterning. By contrast, well-shaped features were observed on the substrate when a stamp with a protruding relief was used for patterning (Fig. 2B). In Fig. 2, AFM topography profiles indicate 2.0 ± 0.3 nm differences between lift-off and non–lift-off areas. The thickness of the TEG SAMs was 1.6 ± 0.1 nm by ellipsometry. The difference can be accounted for by a single atomic layer of Au removed during the lift-off process.

We explored the use of the intact SAM areas as an unconventional resist to transfer patterns to the underlying material, Au, through selective wet chemical etching (*19*, *44*). Exposed areas of the Au surface were contacted by the etchant solution while the intact SAM molecular resist protected the remaining regions of Au. Etchant solutions removed exposed Au via oxidation by Fe^{3+}, followed by complexation and dissolution of oxidized metal by thiourea (*45*). A variety of patterns (inverse replicas of the PDMS stamp features) with features of different sizes were transferred, including lines, holes, and pillars (Fig. 3). The advantages of large patterning areas and high-fidelity features are apparent in the bright-field images (Fig. 3, A to C) and AFM topography images (Fig. 3, D to F), respectively. Differences in AFM heights indicate that features have been transferred to the level of the underlying

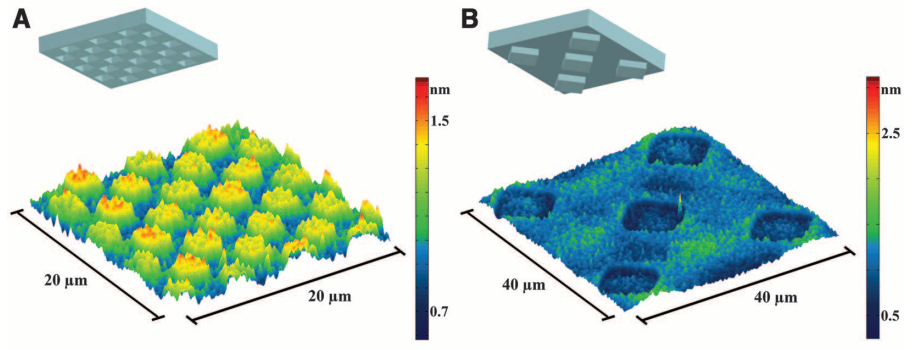

Fig. 2. (**A** and **B**) Atomic force microscope topographic images of substrates patterned by CLL. Self-assembled monolayers of hydroxyl-terminated tri(ethylene glycol)alkanethiol on Au substrates were patterned using CLL and a PDMS stamp with depressed wells (2 μm by 2 μm) (A) or a PDMS stamp with protruding posts (10 μm by 10 μm) (B). Stamp geometries are illustrated above the images. Contact dwell time was 5 min. AFM topographical heights are shown in the scale bars to the right of each image.

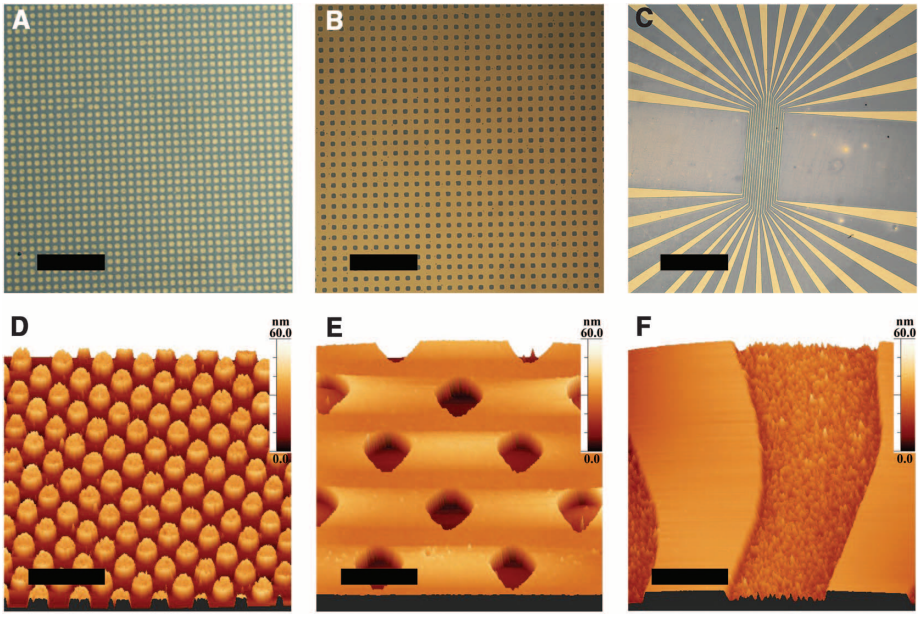

Fig. 3. Patterning underlying gold substrates by CLL. Hydroxyl-terminated tri(ethylene glycol)undecanethiol was self-assembled on Au substrates. Lift-off lithography via activated PDMS stamps was used to produce a variety of patterns. Substrates were then chemically etched (Fe^{3+}/thiourea) to pattern the underlying metal by removing additional gold in the exposed regions. The SAM molecular resist was intact during imaging with bright-field microscopy and AFM. Patterns transferred by the molecular-resist lift-off process include pillars (**A** and **D**), wells (**B** and **E**), and channels (**C** and **F**). Bright-field microscope images are shown in (A) to (C); corresponding AFM topography images are shown in (D) to (F). Scale bars, 18 μm (A), 130 μm (B), 1325 μm (C), 5 μm (D), 15 μm (E), and 17.5 μm (F). AFM topographical heights are shown in the upper right corners of (D) to (F).

substrate at a depth of 30 nm—the thickness of the original Au layer.

In addition to transferring patterns to SAMs and underlying Au substrates, CLL enables a SAM of a different composition to be assembled on the lift-off areas. Figure 4A shows a large-area, high-fidelity pattern of streptavidin binding to a biotinylated pattern created by lifting off areas of an initial TEG SAM to expose fresh Au substrate underneath. The substrate was then exposed to 90:10 TEG/biotin-terminated hexa(ethylene glycol)alkanethiol (Table 1) to produce a low-density biotinylated patterned SAM (*17*, *18*). Streptavidin was captured from solution by surface-tethered biotin. Bound streptavidin was detected by fluorescence microscopy of fluorescein isothiocyanate (FITC)–conjugated antibodies against streptavidin. The bright fluorescent regions in Fig. 4A and its inset display the lift-off areas where biotin-terminated alkanethiols were backfilled and used to capture streptavidin from solution. The dark regions display minimal fluorescence because of the absence of biotin-terminated alkanethiol and the resistance to nonspecific protein adsorption by TEG (*17*, *46*). The fabrication of biotin-streptavidin patterns demonstrates not only that CLL transfers large-area, high-fidelity patterns to SAMs, but also that the Au areas exposed after lift-off are advantageous for producing multiplexed bioselective patterned surfaces.

To carry out nanometer-scale chemical patterning, we implemented the lift-off process for biotin-streptavidin described above, using a PDMS stamp with 90-nm well-like features (Fig. 4B). Areas surrounding the wells were lifted off and backfilled with biotin-terminated alkanethiol to capture streptavidin, whereas the areas inside the wells were not removed, producing TEG islands. In one method to achieve features smaller than 90 nm, a double lift-off strategy was used in which the PDMS stamp was twice brought into conformal contact with the substrate (Fig. 4E). The initial lift-off step removed the molecules in the areas surrounding the stamp wells, leaving the TEG SAM inside the wells intact. During the second lift-off step, the stamp was offset with respect to the first pattern. (This result was initially a serendipitous consequence of being unable to maintain exact registry between multiple stamping steps.) Additional areas of the TEG SAM were removed, depending on the amount of registration. The exposed Au surfaces resulting from both TEG removal steps were backfilled with biotin-terminated alkanethiol. Figure 4E illustrates decreasing registration associated with smaller feature sizes. The resulting intact TEG regions formed increasingly narrow marquise-shaped features with decreased spacing between biotin-streptavidin molecular recognition areas. Note that if conventional contact printing were used in this case, lateral diffusion of ink molecules would blur nanospaced features beyond detection by AFM (*47*). In Fig. 4C, sharp features 40 ± 2 nm in width were directly fabricated using a stamp with 40-nm channels, indicating that we have not yet reached the resolution limit of the CLL method. Exploring the effects of Au grain size will also be important for future mechanistic studies and possible further improvement of nanoscale feature resolution.

Lateral diffusion of ink molecules, which occurs during increasing stamp contact times and/or molecular ink concentrations for additive printing methods on bare Au substrates, is avoided in CLL. Preformed well-ordered SAMs, strong intermolecular interactions between hydrophilic SAM molecules, and a diffusion barrier created by the Au step edges (*48*) formed during lift-off prevent pattern dissolution. Patterned TEG SAMs produced by CLL showed no discernable dissolution after 2 days under ambient storage conditions (fig. S8). Furthermore, the backfilled multicomponent SAMs shown in Fig. 4 were produced by solution

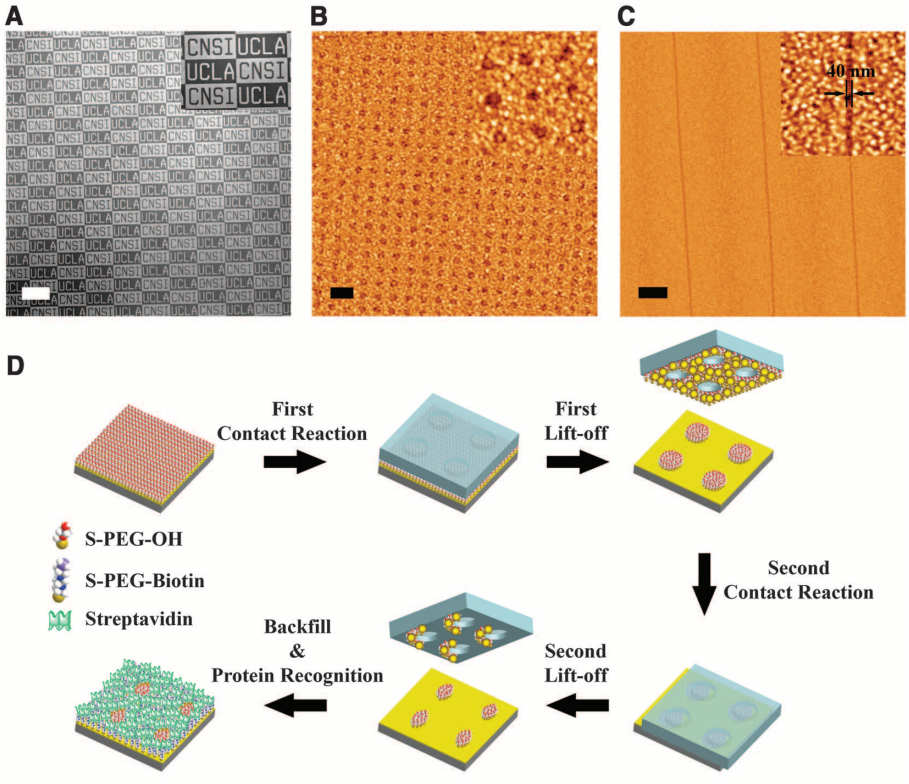

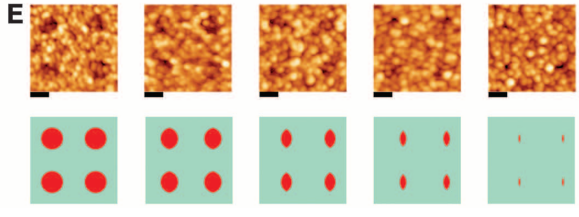

Fig. 4. Large-area patterning of microscale and nanoscale features via CLL. (**A**) Tri(ethylene glycol)alkanethiol (TEG) self-assembled on an Au-coated substrate was subjected to the lift-off process using a PDMS stamp having "UCLA" characters as positive (protruding) features and "CNSI" characters as negative (depressed) features. After patterning, a new monolayer of 90% TEG/10% biotin–terminated oligo(ethylene glycol)alkanethiol (nominal solution ratio) was self-assembled on the exposed Au regions ("UCLA" characters and areas surrounding the "CNSI" characters). Bright areas indicate fluorescence associated with FITC-labeled anti-streptavidin antibody recognition of streptavidin bound to biotin. Dark areas display minimal fluorescence due to the protein-resistant characteristics of TEG. The fluorescent pattern is sharp and extends over a large substrate area (>3 mm^2). Scale bar (main image), 250 μm. (**B**) Au-coated substrates coated with TEG self-assembled monolayers were subjected to the lift-off process using a PDMS stamp with holes 90 nm in diameter. After patterning, a new monolayer of 100% biotin-terminated oligo(ethylene glycol)alkanethiol was self-assembled on the exposed Au regions (areas surrounding the resulting pillar features). Scale bar (main image), 400 nm. The inset shows a high-resolution AFM image of biospecific 90-nm circular features produced by CLL. (**C**) AFM images display biotin-streptavidin recognition areas separated by narrow line features. The inset shows a detailed AFM image of an individual line feature (width 40 ± 2 nm) made using a stamp with 40-nm channels. Scale bar (main image), 1 μm. (**D**) A PDMS stamp with holes 90 nm in diameter was brought into conformal contact once with a TEG SAM (upper left). In this case, substrates were stamped twice with decreasing registry (subsequent images from left to right). Patterned substrates were backfilled with biotin-terminated alkanethiol. (**E**) Topographic AFM images display decreasing feature sizes (from left to right): 90 ± 5 nm, 80 ± 3 nm, 50 ± 2 nm, 30 ± 3 nm, and 15 ± 5 nm. Protruding (lighter) areas indicate biotin-streptavidin recognition. Shallow (darker) areas comprise intact TEG SAM. Scale bars, 100 nm.

deposition of the second SAM component over 12 hours; sharp pattern features were produced even in this case, arguing against diffusion or dissolution of the original lift-off pattern.

We investigated the time needed for the contact-induced chemical reaction at the stamp-substrate interface by examining 1-min versus 5-min contact times between oxygen plasma–treated PDMS stamps and hydroxyl-terminated, alkanethiol-coated Au surfaces. Features were transferred even with 1-min contact times; however, shorter contact times resulted in poor features produced after wet etching. Additionally, pattern transfer was maintained with short SAM deposition times. Hydroxyl-terminated alkanethiol SAMs formed during 1 hour of deposition were found to provide good transfer of stamp features to Au substrates, comparable to transfer obtained from SAMs formed overnight. These findings demonstrate advantages associated with short contact and SAM formation times for facilitating robust, expeditious, and high-throughput patterning by CLL. Ultimately, limits for SAM deposition and stamp contacts times will depend on the specific molecules used for SAM formation.

With this method, conventional nanolithographic patterning techniques such as photolithography and electron-beam lithography need only be used for the fabrication of stamp master molds. Once individual masters are produced, CLL can be implemented as a strategy for high-resolution, high-throughput, low-cost pattern fabrication. Because CLL enables patterns to be transferred to underlying substrates and can be used in a multiple-stamping strategy to produce patterns that are smaller than the actual stamp features, possible applications of CLL include the production of high-fidelity nanometer-scale patterns on Au substrates, as well as patterning of different materials such as Si, Ge, Pd, Pt, and graphene.

References and Notes

1. B. D. Gates *et al.*, *Chem. Rev.* **105**, 1171 (2005).
2. C. G. Willson, B. J. Roman, *ACS Nano* **2**, 1323 (2008).
3. H. M. Saavedra *et al.*, *Rep. Prog. Phys.* **73**, 036501 (2010).
4. W. Shim *et al.*, *Nature* **469**, 516 (2011).
5. R. D. Piner, J. Zhu, F. Xu, S. H. Hong, C. A. Mirkin, *Science* **283**, 661 (1999).
6. S. Xu, P. E. Laibinis, G. Y. Liu, *J. Am. Chem. Soc.* **120**, 9356 (1998).
7. S. Xu, G. Y. Liu, *Langmuir* **13**, 127 (1997).
8. Y. N. Xia, G. M. Whitesides, *Angew. Chem. Int. Ed.* **37**, 550 (1998).
9. X. M. Li, M. Peter, J. Huskens, D. N. Reinhoudt, *Nano Lett.* **3**, 1449 (2003).
10. J. A. Rogers, R. G. Nuzzo, *Mater. Today* **8**, 50 (2005).
11. J. L. Wilbur, A. Kumar, E. Kim, G. M. Whitesides, *Adv. Mater.* **6**, 600 (1994).
12. S. Y. Chou, P. R. Krauss, P. J. Renstrom, *Science* **272**, 85 (1996).
13. Y. L. Loo *et al.*, *J. Vac. Sci. Technol. B* **20**, 2853 (2002).
14. W. R. Childs, R. G. Nuzzo, *J. Am. Chem. Soc.* **124**, 13583 (2002).
15. A. Kumar, G. M. Whitesides, *Appl. Phys. Lett.* **63**, 2002 (1993).
16. K. L. Christman, V. D. Enriquez-Rios, H. D. Maynard, *Soft Matter* **2**, 928 (2006).
17. A. Vaish, M. J. Shuster, S. Cheunkar, P. S. Weiss, A. M. Andrews, *Small* **7**, 1471 (2011).
18. M. J. Shuster *et al.*, *Chem. Commun.* **47**, 10641 (2011).
19. J. M. McLellan, M. Geissler, Y. N. Xia, *J. Am. Chem. Soc.* **126**, 10830 (2004).
20. C. Srinivasan *et al.*, *ACS Nano* **1**, 191 (2007).
21. A. B. Braunschweig, F. Huo, C. A. Mirkin, *Nat. Chem.* **1**, 353 (2009).
22. S. Xu, S. Miller, P. E. Laibinis, G. Y. Liu, *Langmuir* **15**, 7244 (1999).
23. R. C. Tiberio *et al.*, *Appl. Phys. Lett.* **62**, 476 (1993).
24. Y. L. Loo, R. L. Willett, K. W. Baldwin, J. A. Rogers, *J. Am. Chem. Soc.* **124**, 7654 (2002).
25. J. Lahiri, E. Ostuni, G. M. Whitesides, *Langmuir* **15**, 2055 (1999).
26. C. Donzel *et al.*, *Adv. Mater.* **13**, 1164 (2001).
27. T. Kaufmann, B. J. Ravoo, *Polym. Chem.* **1**, 371 (2010).
28. S. R. Wasserman, H. Biebuyck, G. M. Whitesides, *J. Mater. Res.* **4**, 886 (1989).
29. S. J. Stranick, A. N. Parikh, D. L. Allara, P. S. Weiss, *J. Phys. Chem.* **98**, 11136 (1994).
30. S. J. Stranick *et al.*, *Nanotechnology* **7**, 438 (1996).
31. H. Skulason, C. D. Frisbie, *J. Am. Chem. Soc.* **122**, 9750 (2000).
32. M. Liu, N. A. Amro, G. Y. Liu, *Annu. Rev. Phys. Chem.* **59**, 367 (2008).
33. G. E. Poirier, M. J. Tarlov, *Langmuir* **10**, 2853 (1994).
34. G. E. Poirier, M. J. Tarlov, *J. Phys. Chem.* **99**, 10966 (1995).
35. P. Maksymovych, D. C. Sorescu, J. T. Yates Jr., *Phys. Rev. Lett.* **97**, 146103 (2006).
36. M. Yu *et al.*, *Phys. Rev. Lett.* **97**, 166102 (2006).
37. A. M. Moore *et al.*, *J. Am. Chem. Soc.* **129**, 10352 (2007).
38. P. Han *et al.*, *ACS Nano* **3**, 3115 (2009).
39. When oxygen plasma treatment was omitted, a featureless PDMS stamp brought into contact with a hydroxyl-terminated, SAM-coated Au surface failed to produce XPS signature peaks indicative of Au lift-off (fig. S2). Likewise, stamps that were either treated with oxygen plasma or left untreated but not subjected to the lift-off process had no indication of Au on the stamp surfaces (figs. S3 and S4, respectively).
40. H. L. Gou, J. J. Xu, X. H. Xia, H. Y. Chen, *ACS Appl. Mater. Interfaces* **2**, 1324 (2010).
41. O. J. A. Schueller, D. C. Duffy, J. A. Rogers, S. T. Brittain, G. M. Whitesides, *Sens. Actuators A* **78**, 149 (1999).
42. D. C. Duffy, O. J. A. Schueller, S. T. Brittain, G. M. Whitesides, *J. Micromech. Microeng.* **9**, 211 (1999).
43. H. M. Saavedra, C. M. Thompson, J. N. Hohman, V. H. Crespi, P. S. Weiss, *J. Am. Chem. Soc.* **131**, 2252 (2009).
44. W. S. Liao, X. Chen, J. Chen, P. S. Cremer, *Nano Lett.* **7**, 2452 (2007).
45. M. Geissler *et al.*, *Langmuir* **19**, 6301 (2003).
46. K. L. Prime, G. M. Whitesides, *Science* **252**, 1164 (1991).
47. A. A. Dameron *et al.*, *Nano Lett.* **5**, 1834 (2005).
48. S. J. Stranick, M. M. Kamna, P. S. Weiss, *Surf. Sci.* **338**, 41 (1995).

Acknowledgments: Supported by U.S. Department of Energy grant DOE_FG02_10ER46734, NSF grant CHE-1013042, and the Kavli Foundation. S.C. thanks the government of Thailand for a graduate fellowship. We thank D. L. Allara, J. N. Hohman, and S. A. Claridge for helpful discussions; A. Nel for the use of his fluorescent microscope; the California NanoSystems Institute Nano and Pico Characterization Facility; and S. Rujikietgumjorn for help in image processing.

Supplementary Materials

www.sciencemag.org/cgi/content/full/337/6101/1517/DC1
Materials and Methods
Supplementary Text
Figs. S1 to S8
References (*49*, *50*)

12 March 2012; accepted 1 August 2012
10.1126/science.1221774

Pulsating Tubules from Noncovalent Macrocycles

Zhegang Huang,[1,3] Seong-Kyun Kang,[1] Motonori Banno,[2] Tomoko Yamaguchi,[2] Dongseon Lee,[1] Chaok Seok,[1] Eiji Yashima,[2] Myongsoo Lee[1]*

Despite recent advances in synthetic nanometer-scale tubular assembly, conferral of dynamic response characteristics to the tubules remains a challenge. Here, we report on supramolecular nanotubules that undergo a reversible contraction-expansion motion accompanied by an inversion of helical chirality. Bent-shaped aromatic amphiphiles self-assemble into hexameric macrocycles in aqueous solution, forming chiral tubules by spontaneous one-dimensional stacking with a mutual rotation in the same direction. The adjacent aromatic segments within the hexameric macrocycles reversibly slide along one another in response to external triggers, resulting in pulsating motions of the tubules accompanied by a chiral inversion. The aromatic interior of the self-assembled tubules encapsulates hydrophobic guests such as carbon-60 (C_{60}). Using a thermal trigger, we could regulate the C_{60}-C_{60} interactions through the pulsating motion of the tubules.

Self-assembly of small molecular modules into tubules with hollow cavities is a key structural feature of living systems, as exemplified by tobacco mosaic virus and cytoplasmic microtubules (*1*, *2*). Inspired by the biological systems, numerous efforts have been devoted to the design of synthetic building blocks that can form such hollow nanostructures through orchestrated interplay of various noncovalent interactions (*3*). Synthetic tubules have previously been fashioned by self-assembly of lipid molecules (*4*), aromatic amphiphiles (*5*–*9*), and oligopeptides (*10*–*12*). The stacking of ring-shaped compounds is an alternative way to construct tubular structures (*13*, *14*). An example is provided by doughnut-like toroidal proteins that stack on top of one

[1]Department of Chemistry, Seoul National University, Seoul 151-747, Korea. [2]Department of Molecular Design and Engineering, Graduate School of Engineering, Nagoya University, Chikusa-ku, Nagoya 464-8603, Japan. [3]Department of Chemistry, Harbin Institute of Technology, Harbin, 150001, P. R. China.

*To whom correspondence should be addressed. E-mail: myongslee@snu.ac.kr